Maximisation of power density in permanent magnet machines with the aid of optimisation algorithms

Maximization of Power Density in Permanent Magnet Machines with the Aid of Optimization Algorithms

Francesco Cupertino [1], Riccardo Leuzzi [1], Vito Giuseppe Monopoli [1*], and Giuseppe Leonardo Cascella[1]

[1] Department of Electrical and Information Engineering, Politecnico di Bari, via E. Orabona, 4, Bari, Italy
[*] vitogiuseppe.monopoli@poliba.it

Abstract: This paper considers the design of surface-mounted permanent magnet (PM) electrical machines for high-speed applications and proposes a methodology to determine the maximum achievable power density. Power density is usually improved by increasing rotational speed. At high speed, a mechanical retaining system for the rotor magnets must be considered. As the speed increases, the thickness of the retaining sleeve becomes larger, reducing torque capability. There will be an optimal speed at which the output power will be maximized. Both structural and electromagnetic design must be considered simultaneously to properly address this design problem. To simplify the design procedure, static finite-element simulations are used for the electromagnetic analysis and analytical formulas are employed for retaining sleeve sizing. The procedure is aided by multi-objective optimization algorithms. A case study based on the specifications of an aeronautical actuator is presented. The performances that can be obtained using different iron cores, a high-grade silicon steel and a cobalt iron steel, are compared. Finally, results obtained with transient finite-element electromagnetic and structural analysis are presented to validate the feasibility of the proposed procedure.

1. Introduction

In aeronautical and automotive applications, there is a growing interest toward high-speed electrical machines [1], mainly because they allow an increased power density of actuators and generators. This is not only related to the size of the electrical machine, but also to the potential elimination of mechanical gear-boxes, enabling both a weight reduction and system efficiency improvement [2]. Of course, the increase of rotational speed presents issues regarding the structural integrity of the rotor and increased core losses [3]. Additional losses contribute to the temperature increase and eventually introduce deformations and additional mechanical stress. Most of the available brushless machines have been adopted to realize high-speed applications, but permanent magnet (PM) synchronous machines allow the best power-to-weight ratio to be achieved. Such remarkable performances are obtained along with an increase in cost, due to the use of rare earth PM and the rotor complexity because of the need for a PM retaining system. When surface-mounted PM machines are considered, a retaining sleeve is one of the most commonly adopted solutions to ensure rotor integrity [4], [5].

In literature, it is possible to find a number of papers each dealing with the optimization of a particular aspect of permanent magnet machines.

For example, [6] presents a method to widen the high-efficiency range with reasonable computing effort. Indeed, the finite-element method (FEM) is computationally demanding when used to calculate the efficiency. A possible solution to this drawback is represented by the coarse-mesh FEM, which can effectively lower the computational effort by using just a few meshes. The former method can be profitably used with genetic algorithms to shorten the motor design procedure aiming at extending the high-efficiency operating range.

The design procedure proposed in [7] is made faster through the use of nine iteration steps. Each iteration outputs constraints on the machine dimensions using electromagnetic, thermal, and structural analysis. Such outputs are the initial conditions for the subsequent iterations, and based on these constraints, a FEM analysis can be conducted.

In addition, [8] proposed a design method for an interior permanent magnet synchronous generator (IPMSG) made up of consecutive steps with the aim of targeting different objectives (i.e. optimal torque amplitude, torque ripple, and cogging torque). In particular, it tries to take the advantages coming from different design techniques while minimizing the relative drawbacks. First, a sub-optimal solution is obtained through the Taguchi Method. Then, the optimal solution is carried out through a surrogate assisted genetic algorithm (SAGA), which features enhanced computational performances. Finally, the last step improves the optimal solution by considering the effect of the design variable uncertainties. Consequently, the final solution can more closely match the experimental results.

The investigation on such computational aspects is not the only topic that can be found in literature regarding the design procedure. Another topic gathering significant attention is the co-design (i.e. electromagnetic and mechanical) of permanent magnet synchronous machines meant for high-speed applications. In fact, in [9] the design of the stator and of the sleeve was performed through FEM with the aim of lowering the losses, due to the rotor eddy current, as much as possible. Additionally, a more accurate estimation of the iron losses is achieved by considering the influence of harmonics and rotational magnetic flux.

Finally, some design procedures, targeting the cost reduction of permanent magnet synchronous machines, are presented in literature as well. In [10], a multiphysics design method was optimized. In particular, the cost and the efficiency of the converter were also considered to minimize

the overall system cost. The converter losses and costs were kept low through the proper selection of the phase angle of the generator current.

Despite the high number of papers recently published addressing the design of PM machines with the aid of optimization algorithms, none of them considered the maximization of power density as a design objective. Power density is typically increased with the rotational speed, but this limits the torque capability due to the increased size of the mechanical retaining system. To find the speed at which the output power is maximized, the rotational speed is included among the parameters to be optimized, together with stator and rotor geometric parameters, as first suggested in [11] for synchronous reluctance machines. A multi-objective optimization algorithm was adopted to find the best compromise between power density, power factor, and PM quantity. For each machine, the thickness of the retaining sleeve was calculated using analytical formula, and its electromagnetic performances were evaluated using fast magneto-static FEM simulations. The results were validated using detailed transient analysis via finite-element software.

2. Design of high-speed electrical machines

In high-speed electrical machines, magnetic, electrical, and mechanical issues are equally important in determining the final power density. The choice of the magnetic material, the copper and PM quantity, and the structural integrity of the rotor must be considered during the design stage. Recently, multiphysics software solutions based on finite-element analysis capable of considering electrical, magnetic, and mechanical aspects are gaining interest, but they are still time consuming—in particular when coupled to automatic optimisation procedures. In this paper, free software and tools commonly adopted by the scientific community are preferred to solve the multiphysics design problem. In particular, finite-element method magnetics (FEMM) software [12] is used to analyse the electromagnetic behaviour of the machines with magneto-static FEM analysis. This software integrates a scripting feature in Matlab that allowed us to couple FEMM with an optimisation algorithm written in Matlab language. The realisation of the FEM model, the execution of the optimisation procedure, and the post processing of the results is handled with the open-source suite SyR-e [13]. SyR-e includes a lumped parameter thermal model that can predict the steady-state copper temperature for a given distribution of Joule losses. The maximum admissible Joule losses are then determined on the basis of the copper steady-state temperature. Then, the stator current is automatically adjusted to keep the stator Joule losses constant.

The software also includes a simplified analytical model to calculate the thickness of a retaining sleeve by considering the rotor geometry and rotational speed, as will be described in detail later.

2.1. Motor parameterization

Among the parameters that affect the performance of PM machines the most are the motor volume, current density, and PM quantity. In this work we will consider motor volume as a constrain, taking its value from the specification of an aeronautical actuator. Regarding the stator slots, higher numbers usually guarantee a reduced harmonic content in the stator magneto-motive force, and this can have a beneficial effect in reducing iron losses. The number of poles should be kept low to limit the electrical frequency in high-speed applications. A combination of 24 stator slots and 4 rotor poles was considered here because it is recognized as a good compromise among the conflicting goals mentioned above.

Regarding the current density, it was selected to keep the ratio k_j between the stator Joule losses and the outer stator stack surface constant. This value, measured in kW/m^2, is a measure of the electric loading of the machine and typically ranges between 3 kW/m^2 for naturally cooled machines up to 30 kW/m^2 for liquid-cooled machines. During the optimization process, for each machine to be evaluated, the stator resistance is estimated first and then the current that gives the desired k_j value is calculated. This is the current value used during the FEM evaluation to evaluate motor performance. This means that, during a single optimization run, all the machines will be evaluated to keep the Joule losses constant.

The main geometrical parameters describing stator and rotor geometry, namely the tooth width (t_w) and length (t_l), the rotor radius (r_{SL}) and PM thickness (l_{PM}) as described in Figure 1, together with the rotational speed, are the parameters selected by the optimization algorithm.

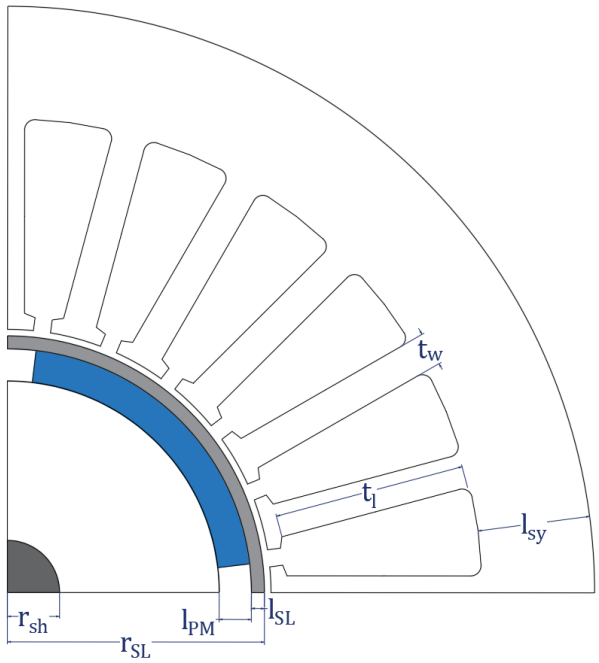

Fig. 1. *Main parameters of stator and rotor geometries.*

2.2. Automatic calculation of retaining sleeve thickness

To properly select the sleeve thickness, the overall tangential stress (also known as hoop stress) acting on the sleeve is calculated. Then, the sleeve thickness is selected to ensure that the total hoop stress does not exceed the yield stress limit of the sleeve material.

To obtain a simple model, we assume that the total hoop stress on the sleeve is only due to two factors, namely the centrifugal force produced by the permanent magnets and the inertial stress due to the mass of the sleeve.

We are not considering here the effects of temperature and interference fit that will be used to transfer the torque among rotating parts. The impact of such phenomena will be evaluated at the end of the design procedure using finite-element software. The main aim here is to obtain an approximate model to predict the sleeve thickness and evaluate its impact on electromagnetic performance.

The centrifugal stress on the sleeve due to the magnets can be calculated as

$$\sigma_{t,PM} = \frac{\frac{F_{c,PM}}{2\pi C_{PM}} C_{SL}}{L_{PM} l_{SL}}, \quad (1)$$

where $F_{c,PM} = N_{PM} m_{PM} C_{PM} \omega_{max}^2$ is the centrifugal force due to the magnets (N_{PM} is the PM number, m_{PM} is the mass of each magnet, and ω_{max} is the maximum rotating speed of the machine); C_{PM} and C_{SL} are the radii of the mass centres of magnets and sleeve, respectively; L_{PM} is the axial PM length; and l_{SL} is the sleeve thickness in the radial direction.

The inertial stress due to the sleeve mass itself has again a centrifugal nature (i.e. it is proportional to the square of the speed). With the assumption of the sleeve thickness being much smaller than its diameter, the inertial stress of the sleeve can be calculated as

$$\sigma_{t,SL} = \gamma_{SL} C_{SL}^2 \omega_{max}^2, \quad (2)$$

with γ_{SL} being the specific density of the sleeve material.

Due to the inaccuracy of the simplified model, a safety factor $K_s = 2$ has been introduced for the maximum stress value tolerated by the sleeve material [14]. The total sleeve hoop stress $\sigma_{SL} = \sigma_{t,PM} + \sigma_{t,SL}$ must be less than or equal to the yield strength of the material divided by the safety factor:

$$\frac{\frac{F_{c,PM}}{2\pi C_{PM}} C_{SL}}{L_{PM} l_{SL}} + \gamma_{SL} C_{SL}^2 \omega_{max}^2 \leq \frac{\sigma_{y,SL}}{K_s}. \quad (3)$$

From (3), it is possible to calculate the minimum required sleeve thickness as in (4):

$$l_{sl} = \frac{N_{PM} m_{PM} r_{SL} \omega_{max}^2}{\pi L_{PM} \left[\frac{\sigma_{y,SL}}{K_s} - \gamma_{SL} r_{SL}^2 \omega_{SL}^2\right]}, \quad (4)$$

where the outer rotor radius $r_{SL} = r_{FE} + l_{PM} + l_{SL}$ is used in place of both C_{PM} and C_{SL}. This assumption simplifies the sleeve thickness calculation and leads to more conservative results.

Optimization algorithms

Meta-heuristic optimization algorithms use a set of candidate solutions (population) that are iteratively modified according to probabilistic rules aimed at finding the global minimum of the chosen objective (or cost) function. The reader who is interested in a more detailed description may refer to [15]. It has been demonstrated that there does not exist any single algorithm that is the best for any class of search problems (no free-lunch theorem [16]), and no algorithm can avoid the risk of convergence to suboptimal solutions. For most practical problems, this is no real limit since the user is usually looking for a solution that satisfies the problem requirement and has limited time for the design stage. Differential evolution (DE) algorithms represent a good compromise between simplicity and effectiveness in a large class of optimization problems [17].

All meta-heuristic algorithms can solve multi-objective problems by introducing the concept of dominance. A solution is non-dominated when there is no other solution having better values for all the cost functions or objectives. We adopted the approach proposed in the NSGA-II algorithm for non-dominated and crowding distance sorting [18].

At each iteration of the multi-objective algorithm, it is possible to determine the subset of non-dominated solutions in the current population—this subset is called the Pareto front. Solutions belonging to this Pareto front are equally good for the multi-objective problem. At the end of the optimization procedure, the interaction is requested with the designer, who must select the most adequate solution, knowing how much each cost function has to be sacrificed in order to favour the others. The best compromise between competitive cost functions can only be a human choice. Multi-objective optimization algorithms are a powerful tool to analyse and solve optimization problems in engineering design applications. However, the computational burden of the optimization procedure and the complexity of the analysis of the results rapidly grows with the number of cost functions. In this paper we have limited to two the number of cost functions, while the other design objectives are considered by introducing some penalty factors, as described in the next section.

2.3. Selection of cost functions

One of the two cost functions will always be the output power, since the maximization of the power density is the main objective of the electromagnetic design considered here. Since the optimization algorithm is written for minimization problems, the output power is multiplied by -1. As second cost function, the quantity of permanent magnet or the power factor could be considered. The copper quantity is determined with the choice of k_j parameter that determines the ratio between Joule losses and stator outer surface. Among other potential cost functions, minimization of torque pulsations or winding configurations have limited impact on the power density. Power factor and PM quantity are the most critical objectives because the minimization of the former and the maximization of the latter favour the increase of power density. In the design of high-speed machines, solutions tend to have poor power factor when the PM quantity is minimized and tend to use the largest possible PM quantity when the power factor is considered as an objective function to be maximized. To avoid a three-objective run (considering power, PM quantity, and power factor as objectives), two approaches are suggested here. In a first set of optimization runs, power and PM quantity are considered as objectives, and a penalty factor is applied to the machines which have a power factor below a predetermined threshold (hereinafter P/PM run). The penalty consists of applying a factor 1/10 to the torque and a factor of 10 to the PM quantity when the power factor is not satisfactory. Such penalized solutions become sufficiently far from the Pareto front and will be discarded by the optimization algorithm. This first set of optimizations is used to select the PM quantity. Then, a second set of optimization runs is performed using power and power factor as objectives and fixing the PM quantity to a predetermined value (hereinafter P/IPF run). In this case, the optimization algorithm will select the PM thickness, but its angular span will be adapted so to keep the PM quantity constant.

3. Design problem statement

As a design example, the specifications of a high-speed actuator designed for aeronautic applications were considered to define the machine volume and a reasonable range for its torque and speed. Required continuous power for the original actuator was 50 kW at a base speed of 50.000 rpm, and the maximum overload power was equal to 75 kW. Its outer stator diameter was equal to 90 mm, the active axial length of the machine was 120 mm, and the airgap was 0.5 mm. Adopting a k_j index of about 30 kW/m^2 gives in this case a value of admitted Joule losses of about 1 kW. The copper over-temperature with respect to the cooling water was estimated to be equal to 60°C using a lumped-parameter thermal network. A titanium alloy was considered for the retaining sleeve.

The lamination parameters most affecting the performances of high-speed machines are the saturation flux density and the iron losses. To determine the most suitable lamination material to realize high-speed PM machines, a cobalt-iron (CoFe) and a silicon-iron (SiFe) alloy were considered here. Each material excels in one of the features mentioned above (i.e. flux density or losses). The main lamination properties are summarized in Table 1. The CoFe material was considered thermally treated for maximizing its magnetic properties (Vacodur49 "opt. mag."). Vacodur49 is produced by Vacuumschmelze and will be referred to as Vac in the following [19]. The SiFe alloy considered here is the 10JNEX900 (hereinafter referred to as Jnex) produced by JFE Steel Corporation with a lamination thickness of 0.1 mm, a lower saturation flux density (around 1.5 T), yield strength around 600 MPa, and reduced core losses [20].

3.1. Settings for the optimization algorithm

The main specific parameters to be selected before running a DE algorithm are the mutation factor F, and the crossover rate C_r that determine the balance between exploitation of the available information and exploration of the search space. As first, as suggested in [21], F was randomly selected in the range [0, 1.5] while C_r was selected to be equal to 0.95. Other parameters that characterize all population-based optimization algorithms are the population size, here selected to be ten times higher than the number of parameters to be optimized, and the maximum number of iterations, here selected at 1.2 times the population size and used as a stopping criterion for the optimization procedure. Since the parameters to be optimized are five (namely tooth width and length, rotor radius, PM thickness, and rotational speed), 50 individuals were iterated for 60 generations at each optimization run. The limits of the search space are reported in Table 2. It is important to emphasize that a check for the feasibility of the motor geometry is unavoidable, in particular when FEA are included in the objective function evaluation. The presence of very close lines or sharp angles could compromise the convergence of FEA and reliability of the results. For example, in this work when the combination of the stator parameters does not guarantee a minimum stator yoke thickness (i.e. 5 mm), the stator tooth length is automatically reduced.

Table 1 Electrical and mechanical properties of the iron alloys

Lamination Type	Vacodur49	10JNEX900	Unit
Loss @ 50 Hz, 1.5 T	1.6	1.47	[W/kg]
Loss @ 400 Hz, 1.5 T	31.0	14.0	[W/kg]
Loss @ 1000 Hz, 1.5 T	150	46.6	[W/kg]
Loss @ 2000 Hz, 1.5 T	390*	118.8	[W/kg]
Yield strength	390	604	[MPa]
Mass density	8120	7490	[kg/m3]

* Extrapolated values

Table 2 Limits of the search space

Parameter	Bounds
Rotor radius, mm	[14 24]
PM thickness, mm	[1.3 4]
Tooth width, mm	[1.8 3.5]
Tooth length, mm	[12 19]
Rotational speed, krpm	[30 100]

4. Results

As mentioned in the previous section, two sets of optimization runs were executed. In the first set, hereinafter referred as P/PM run, the objective functions are the output power and magnet quantity. The magnet quantity was measured with the area of a single magnet, in square millimetres. Note that all the considered machines have four poles and an axial length equal to 120 mm: then, the single PM section is representative of the total PM quantity. The second set of optimization runs considered output power and internal power factor as objective functions and is hereinafter referred to as P/IPF run. The internal power factor is defined as the cosine of the phase angle between the back-electromotive force and the stator current. We will consider surface-mounted PM machines operated with the stator current in quadrature to the PM flux linkage. In this case, the internal power factor can be defined as in (5):

$$\mathrm{IPF} = \cos\left(\arctan\left(\frac{\lambda_q}{\lambda_d}\right)\right) = \cos\left(\arctan\left(\frac{L_q i_q}{\psi_{PM}}\right)\right), \qquad (5)$$

where $\lambda_d = L_d i_d + \psi_{PM}$ and $\lambda_q = L_q i_q$ are the d- and q-axis flux linkages. The calculation of the IPF is preferred here because it does not need the knowledge of motor losses, which are difficult to estimate using magnetostatic FEM software (e.g. iron and sleeve losses), but it is representative of the final power factor (PF). Machines with higher IPF will generally have higher PF.

The first optimization results were obtained with P/PM runs, applying a penalty factor to machines having an IPF lower than 0.7 (see Figure 2) and 0.8 (see Figure 3). Maximum PM quantity in the Pareto front machines is greater when the requested power factor is higher, but it never reaches the maximum allowable PM quantity within the search space. In the considered runs, there is an amount of magnet beyond which the increase of the thickness of the sleeve would penalize the performances in terms of

electromagnetic torque eliminating the positive effect of the increased PM quantity. These results allow to determination of the ideal PM quantity for the considered machine to maximize power density. PM area close to 300 mm^2 gives the higher power density, but PM area between 200 mm^2 and 250 mm^2 seems to ensure the most effective use of the magnet quantity. Above 250 mm^2, the increase of power is less pronounced. There is a loss in output power at the same PM quantity going from 0.7 to 0.8 IPF machines. This loss could be approximately quantified around 10% with high PM quantity (e.g. over 250 mm^2) and around 30% with reduced PM quantity (e.g. below 150 mm^2). Another interesting result is the advantage of Vac machines over Jnex machines of approximately 10 kW at the higher PM quantity. This advantage tends to disappear when the machines have a lower magnetic loading with reduced PM quantity. The Pareto fronts obtained with different lamination material tend to overlap below 170 mm^2 of PM area. The cross-sections of the machines reveal larger stator iron paths for the machines with IPF equal to 0.8. The Vac machines have, in general, reduced tooth thickness, thanks to the higher saturation flux.

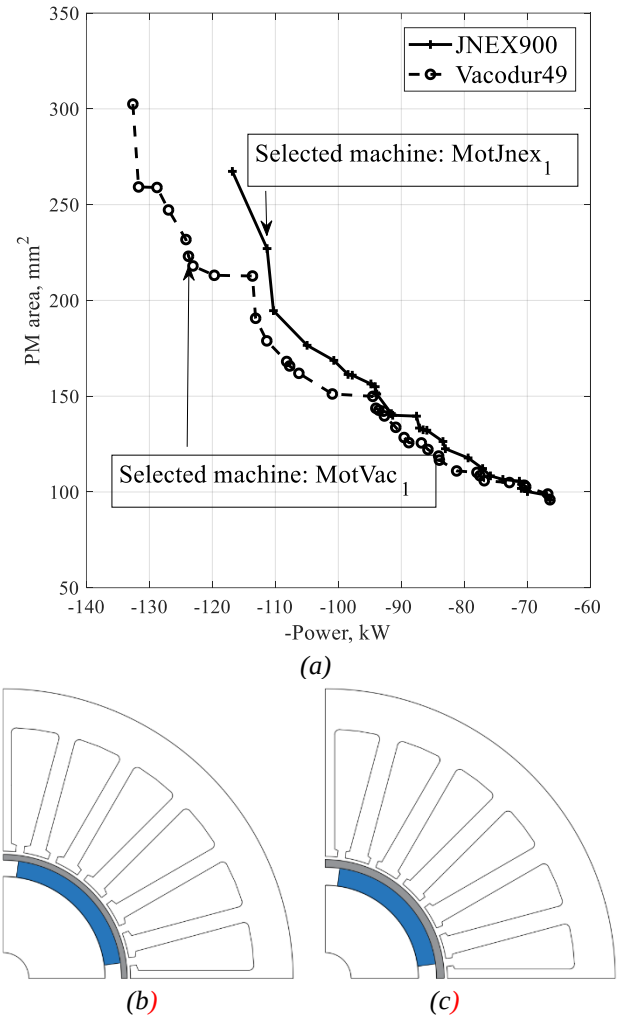

Fig. 2. *P/PM run with penalty factor for IPF below 0.7: Pareto fronts obtained using Jnex900 (solid) and Vacodur49 (dashed) steel (a), and cross-section of selected machines MotJnex$_1$ (b) and MotVac$_1$ (c).*

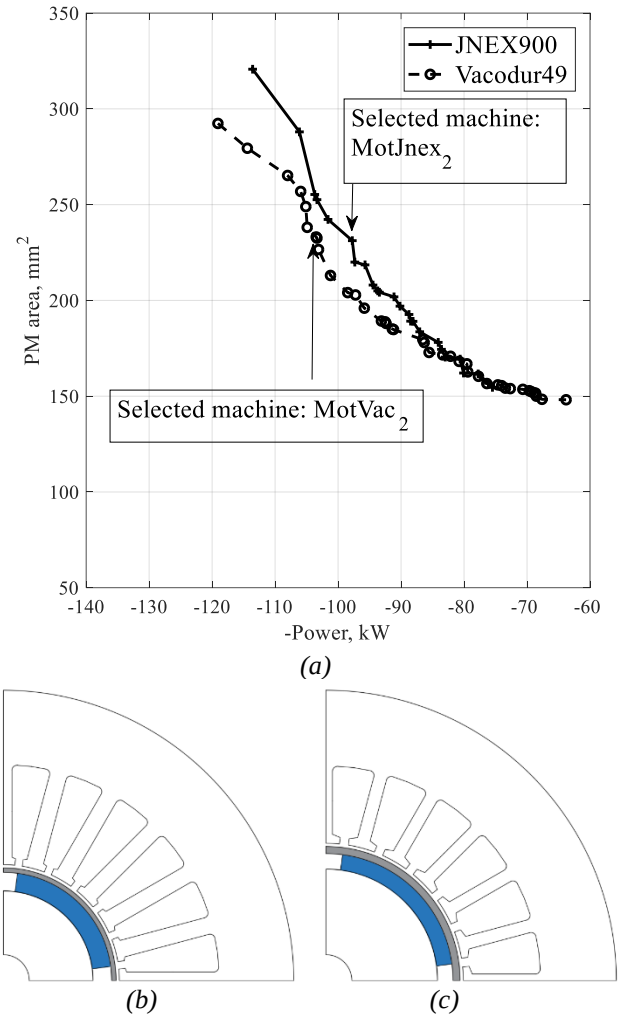

Fig. 3. *P/PM run with penalty factor for IPF below 0.8: Pareto fronts obtained using Jnex900 (solid) and Vacodur49 (dashed) steel (a), and cross-section of selected machines MotJnex$_2$ (b) and MotVac$_2$ (c).*

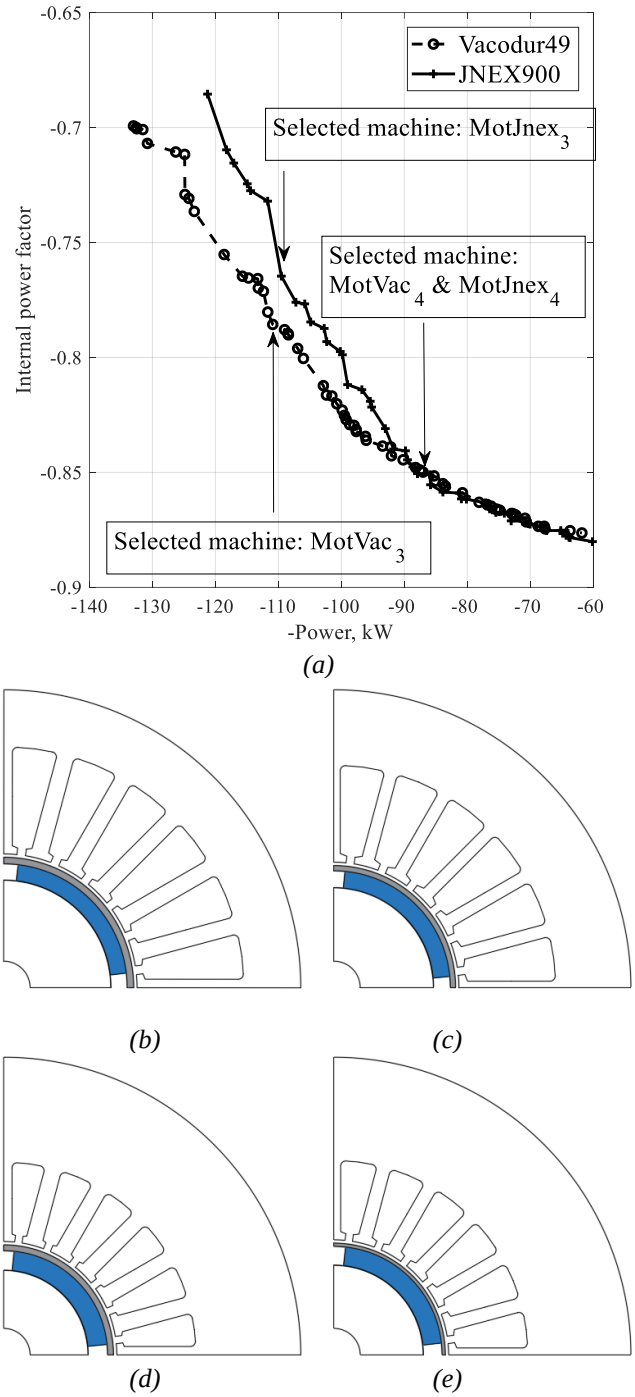

Fig. 4. *P/IPF run with PM quantity equal to 230 mm2: Pareto fronts obtained using Jnex900 (solid) and Vacodur49 (dashed) steel (a), and cross-section of selected machines MotJnex₃ (b), MotVac₃ (c), MotJnex₄ (d), MotVac₄ (e).*

After the analysis of these results, the PM area was set at 230 mm^2, a value considered to be a good compromise between achievable performances and cost of the machines, and a P/IPF optimization run was performed. The results are reported in Figure 4. In this case, four machines were selected from the Pareto fronts, with approximately 110 kW output power, and the other two with about 85 kW. Again, machines with a low magnetic loading have thicker stator iron paths, higher power factor, and similar performances between Vac and Jnex machines.

Table 3 Geometric parameters of the selected optimized machines

Parameter	MotJnex$_3$	MotVac$_3$	Unit
Axial length	120	120	mm
Stator outer radius	45	45	mm
Airgap	0.5	0.5	mm
Rotor radius	19.7	18.4	mm
PM thickness	2.5	2.6	mm
Tooth width	2.6	2.0	mm
Tooth length	16.2	14.7	mm
Sleeve thickness	1.0	0.8	mm

This is confirmed by the lower part of the Pareto fronts, which is overlapped in Figure 4 for Jnex and Vac machines. Reducing the IPF from 0.85 to the 0.75-0.8 range allows a considerable increase of output power. The selection of IPF value should consider the power converter sizing in addition to the electromagnetic performance of the machine. Because this analysis is beyond the scope of this paper, here IPF above 0.75 is considered the minimum requirement, and machines MotJnex$_3$ and MotVac$_3$ were selected for detailed validation of the results. Table 3 reports the main geometric parameters of the selected machines.

5. Validation of results and discussion

The machines designed and selected in the previous section, namely MotVac$_3$ and MotJnex$_3$, were analysed using transient finite-element software to validate both the electromagnetic and mechanical designs by analysing the losses breakdown and the distribution of mechanical stress. If such detailed analysis tools were adopted during the optimization stage, the computational burden would increase by an order of magnitude. A single machine evaluation performed using FEMM software requires a few seconds on a laptop Windows PC. Then, a single optimization run is completed in a couple of hours. On the other hand, both transient electromagnetic analysis with Magnet software [22] and mechanical analysis with Ansys [23] software required several minutes on a Xeon-based workstation for a single machine evaluation.

5.1. Electromagnetic analysis

The main results of the electromagnetic analysis are summarized in Tables 4 and Table 5, considering rated and overload conditions. In the tables, the rotor losses were calculated by considering the sleeve and magnet segmentation in the axial direction. This is a commonly adopted solution to mitigate the losses due to rotor parasitic currents in conducting materials. This choice also simplifies the rotor manufacturing process since each sleeve or magnet section has reduced axial length and, consequently, has fewer problems with locking during assembly. The losses into the sleeve, including the segmentation, were calculated starting from a 2D electromagnetic analysis and considering the theory presented in [24]. The sleeve losses are approximated by the following formula:

$$Sleeve\ losses = \left[1 - \frac{\tanh\left(\frac{n_p L_{sec}}{D}\right)}{\frac{n_p L_{sec}}{D}}\right] P_{sleeve2D}, \qquad (6)$$

where $P_{sleeve2D}$ is the sleeve power loss obtained, neglecting the tangential paths of the parasitic currents, L_{sec} is the axial length of a single sleeve section, and D is its diameter. Without segmentation, sleeve losses would be approximately 1 kW. We calculated that ten segments allow a loss reduction down to 100 W and used this value for the analysed machines. It should be noted that because sleeve losses are comparable for selected machines, they do not play a significant role in the performance comparison. Thanks to the shielding effect of the conducting sleeve, the losses into the magnets and rotor iron were found to be negligible.

The machines have the same 1000 W of Joule losses at rated conditions, which is the value considered during the optimization stage. The $MotVac_3$ machine has a rated speed of 75.472 rpm, while the $MotJnex_3$ has a rated speed of 76.521 rpm. Despite the higher frequency, the stator losses of $MotJnex_3$ are lower. The efficiency of the two machines is comparable and above 98%. $MotJnex_3$ has a small advantage in terms of efficiency, both at rated and overload conditions, primarily due to the reduced stator iron losses.

If other machines were selected from the previous Pareto fronts, having reduced magnetic loading (i.e. lower PM quantity or higher IPF), the advantage of the Jnex machines in terms of power-to-loss ratio would be more evident.

Figure 5 reports the torque versus rotor position characteristic calculated for the selected machines. The peak-to-peak torque ripple is always 10% below the average torque both at rated and overload conditions. At rated current, the torque ripple is 8% for $MotJnex_3$ and 7% for $MotVac_3$. These results show that no particular care must be dedicated to the torque ripple reduction, since 10% is an admissible limit in many applications. If lower torque ripple values were requested it could be possible to introduce a penalty factor for machines with high torque ripple, as done with IPF in the P/PM run.

In conclusion, it can be stated that both considered lamination materials are suitable for the considered high-speed application, and there is no evident winner out of the comparison in rated operative conditions.

Table 4 Performances of the selected optimized machines at rated conditions

Parameter	$MotJnex_3$	$MotVac_3$	Unit
Current	23.2	22.6	Apk
Rated speed	76521	75472	rpm
Rated frequency	2551	2514	Hz
d-axis flux	0.195	0.205	Wb
q-axis-flux	0.166	0.162	Wb
Torque	13.4	13.7	Nm
Output power	108.9	108.3	kW
Copper losses	1000	1000	W
Stator iron losses	415	729	W
Rotor iron losses	0	0	W
Magnet losses	1	1	W
Sleeve losses	109	98	W
Total losses	1525	1828	W
Efficiency	98.6	98.3	--
Int. power factor	0.76	0.79	--

They reach comparable power densities when the magnetic material is adequately loaded, which is a usual condition in high-speed applications. Conversely, the Jnex machines can benefit from the reduced iron losses with improved efficiency in light load conditions. This advantage could be crucial in some applications.

Table 5 Performances of the selected optimized machines at overloaded conditions

Parameter	$MotJnex_3$	$MotVac_3$	Units
Current	34.8	33.9	Apk
Rated speed	76521	75472	rpm
Rated frequency	2551	2514	Hz
d-axis flux	0.180	0.190	Wb
q-axis-flux	0.227	0.222	Wb
Torque	18.5	19.0	Nm
Output power	148.0	150.0	kW
Copper losses	2250	2250	W
Stator iron losses	545	966	W
Rotor iron losses	0	0	W
Magnet losses	2	2	W
Sleeve losses	181	178	W
Total losses	2978	3396	W
Efficiency	98.0	97.8	--
Int. power factor	0.62	0.65	--

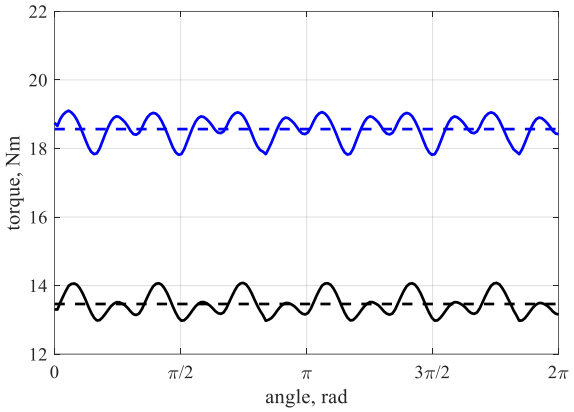

(a)

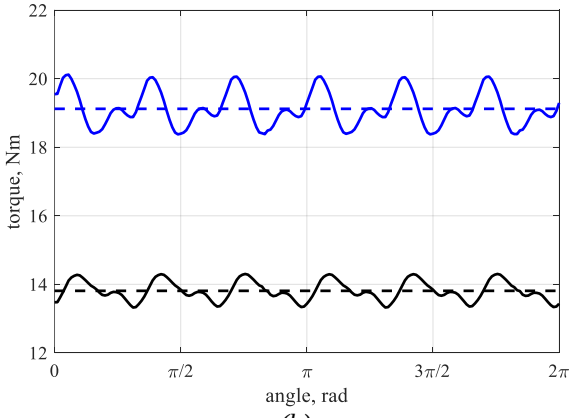

(b)

Fig. 5. *Torque waveforms of selected machines $MotJnex_3$ (a) and $MotVac_3$ (b) calculated at rated (black line) and overload (blue line) conditions.*

5.2. Mechanical analysis

To validate the sleeve sizing procedure presented in section 2 and to verify the feasibility of the selected machines, several structural FEA simulations were performed with the Ansys software. A planar cross-section of the rotor with quadratic mesh elements was analysed to calculate the overall stress acting on the sleeve. We checked the mechanical stress in two extreme working conditions, namely at standstill with minimum ambient temperature (-55°C) and at rated speed with maximum ambient temperature (+85°C). The results are reported in Figure 6. The most severe operating condition is the one at rated speed and maximum temperature for all the analysed machines. The maximum von Mises stress is approximately 600 MPa at standstill and 770 MPa at rated speed. Considering that the yield strength of the sleeve material is equal to 1100 MPa (Inconel 718 titanium alloy), the actual safety factor is between 1.5 and 1.8 in the considered operating conditions. The maximum stress values are reached at rated speed only in small portions of the sleeve, in between the magnets, which is the region with higher deformations. The presence of some filling material between the magnets, as would be the case with inset magnets, would reduce sleeve deformations and consequently mitigate the peak stress values. It is evident that the approximated mechanical model underestimates the actual stress because it considers and accurately predicts the average stress condition of the sleeve but does not include all the stress contributions, such as those induced by local deformation. Also considering these limitations, the approximated mechanical model is adequate to compare different designs during the optimization procedure, and the model inaccuracy can be effectively compensated using a slightly higher safety factor.

It must be ensured that there is no loss of contact between PMs and sleeve in more severe working conditions. The contact condition is satisfied if the pressure on the contact area between magnets and sleeve, calculated via FEA considering the interference fit between the two parts, is higher than the minimum required pressure to transfer the maximum torque at the maximum speed. The minimum required pressure can be calculated as in (7):

$$p_{min} = \frac{S\,F_N}{\beta_{PM} L_{PM}} \tag{7}$$

where β_{PM} is the arc length of the contact area between a PM and the sleeve, F_N is the radial force required to transmit the torque, and S is a safety factor that has been set to 1.5. The radial force F_N is calculated as in (8):

$$\mathrm{F_N} = \frac{\mathrm{F_T}}{\mathrm{f}} = \frac{\mathrm{T_{max}}}{\mathrm{N_{PM} R_{PM} f}} \tag{8}$$

where F_T is the tangential force given by the maximum torque (T_{max}) divided by the number of magnets (N_{PM}) and by the radius at the contact area (R_{PM}), and f is the friction coefficient.

To take into account the interference fit within the simulation, an equivalent negative thermal gradient, calculated to ensure torque transmission, was imposed on the sleeve component in the model. As an example, the analysis of the pressure distribution for MotVac$_3$ is shown in Figure 7, calculated at maximum speed and temperature. The minimum required pressure is 0.5 MPa, and the contact condition is clearly satisfied.

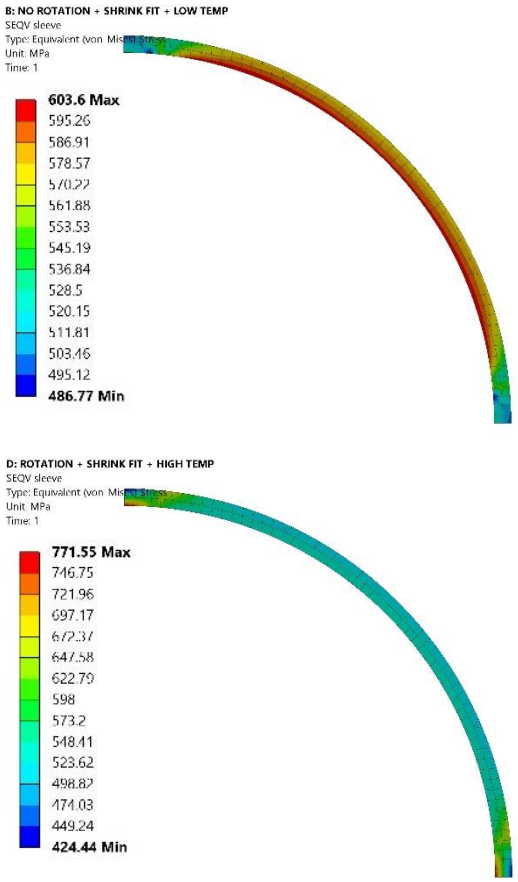

Fig. 6. *Mechanical analysis to verify the sleeve stress distribution at (a) standstill with minimum temperature and (b) rated speed and maximum temperature for MotVac$_3$.*

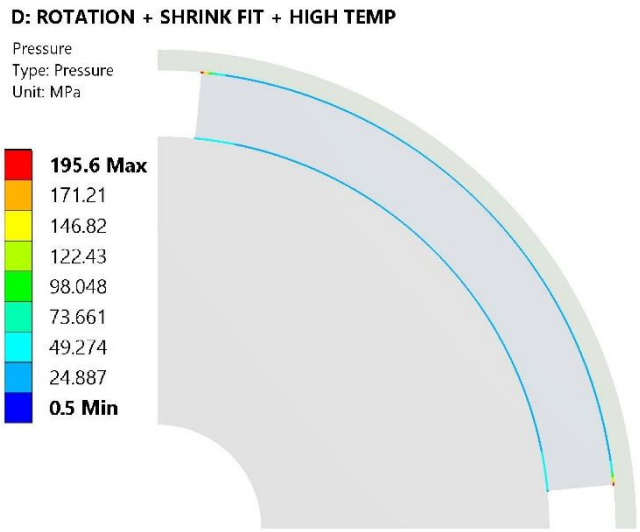

Fig. 7. *Mechanical analysis to verify the minimum contact pressure at maximum speed and temperature for MotVac$_3$.*

6. Conclusion

In this paper, the maximization of the power density of a synchronous PM machine is reviewed as an optimization problem. With the aim to reduce the computational burden, the proposed design procedure employs static finite-element simulations for electromagnetic analysis and a simplified mechanical analytical model for the sleeve thickness sizing.

A two-step optimization procedure is presented to maximize the power density of a PM machine. The first step uses power and PM quantity as cost functions and enables selection of the optimal PM quantity. The second step uses power and IPF as cost functions with a fixed PM quantity and allows the selection of the final design. The proposed procedure provides a balance among maximum power density, PM quantity, and IPF within the design specifications.

The use of both a high-flux-density cobalt-iron and a low-loss silicon-iron alloy is considered and the respective performances compared. The results reveal that the power density at a given loss level is comparable with both lamination materials. A clear advantage of silicon-iron machines is seen when the magnetic loading of the machines is reduced or in light load operating conditions.

The guidelines presented here can be easily extended to other design problems by changing the machine specifications and using the simple models or free software tools described here.

7. References

[1] Rahman, M.A., Chiba, A., Fukao, T.: "Super high speed electrical machines - summary". Proceedings of the IEEE Power Engineering Society General Meeting, vol. 2, pp. 1272, 1275, 6-10 June 2004.

[2] Gerada, D., Mebarki, A., Brown, N. L., Gerada, C., Cavagnino, A., Boglietti, A.: “High-Speed Electrical Machines: Technologies, Trends, and Developments”. IEEE Transactions on Industrial Electronics, vol. 61, no. 6, pp. 2946-2959, June 2014.

[3] Borisavljevic, A., Polinder, H., Ferreira, J. A.: "On the Speed Limits of Permanent-Magnet Machines". IEEE Transactions on Industrial Electronics, vol. 57, no. 1, pp. 220-227, Jan 2010.

[4] Binder, A., Schneider, T., Klohr, M.: "Fixation of buried and surface-mounted magnets in high-speed permanent-magnet synchronous machines". IEEE Transactions on Industry Applications, vol. 42, no. 4, pp. 1031-1037, July-Aug. 2006.

[5] Krahenbuhl, D., Zwyssig, C., Weser, H., Kolar, J.W.: “A Miniature 500 000-r/min Electrically Driven Turbocompressor”. IEEE Transactions on Industry Applications, vol. 46, no. 6, pp. 2459-2466, Nov-Dec 2010.

[6] Nakata, T., Sanada, M., Morimoto, S., Inoue, Y.: “Automatic design of IPMSMs using a genetic algorithm combined with the coarse-mesh finite element method for enlarging the high-efficiency operation area”. IEEE Transactions on Industrial Electronics, vol. 64, no. 12, pp. 9721–9728, Dec. 2017.

[7] Uzhegov, N., Kurvinen, E., Nerg, J., Pyrhönen, J., Sopanen, J.T., Shirinskii, S.: “Multidisciplinary Design Process of a 6-Slot 2-Pole High-Speed Permanent-Magnet Synchronous Machine”. IEEE Transactions on Industrial Electronics, vol. 63, no. 2, pp. 784–795, Feb. 2016.

[8] Lim, D. K., Jung, S. Y., Yi, K. P., Jung, H. K.: “A novel sequential-stage optimization strategy for an interior permanent magnet synchronous generator design”. IEEE Transactions on Industrial Electronics, vol. 65, no. 2, pp. 1781–1790, Feb. 2018.

[9] Zhang, Y., McLoone, S., Cao, W., Qiu, F., Gerada, C.: “Power Loss and Thermal Analysis of a MW High-Speed Permanent Magnet Synchronous Machine”. IEEE Transactions on Energy Conversion, vol. 32, no. 4, pp. 1468–1478, Dec. 2017.

[10] de Paula Machado Bazzo, T., Kölzer, J.F., Carlson, R., Wurtz, F., Gerbaud, L.: “Multiphysics design optimization of a permanent magnet synchronous generator”. IEEE Transactions on Industrial Electronics, vol. 64, no. 12, pp. 9815–9823, Dec. 2017.

[11] Cupertino, F., Palmieri, M., Pellegrino, G.: “Design of high-speed synchronous reluctance machines”, Proceedings of IEEE ECCE 2015, Energy Conversion congress & EXPO. Montreal (Canada), 20-24 September 2015, pp. 4828-4834.

[12] Finite Element Method Magnetics. Available online: http://www.femm.info/wiki/HomePage (accessed on December 25 2017).

[13] Syre—Synchronous Reluctance (Machines) Evolution. Available online: http://sourceforge.net/projects/syr-e/ (accessed on December 25 2017).

[14] Lahne, H. C., Gerling, D., Staton, D., Chong, Y. C.: “Design of a 50000 rpm high-speed high-power six-phase PMSM for use in aircraft applications”, Proceedings of Eleventh International Conference on Ecological Vehicles and Renewable Energies (EVER), 6-8 April 2016, Montecarlo, Monaco.

[15] Goldberg, D. E.: “Genetic Algorithms in search, optimization, and Machine Learning”, 1st ed., Addison-Wesley: Boston, MA, USA, 1989; ISBN: 0201157675.

[16] Wolpert, D. H.; Macready, W. G.: “No Free Lunch Theorems for Optimization”. IEEE Transactions on Evolutionary Computation, vol. 1, no. 1, pp. 67-82, Apr 1997.

[17] Neri, F.; Tirronen, V.: “Recent advances in differential evolution: A survey and experimental analysis”. Artificial Intelligence Review, vol. 33, no. 1–2, pp. 61–106, Feb 2010.

[18] Deb, K., Pratap, A., Agarwal, S., and Meyarivan T.: “A Fast and Elitist Multiobjective Genetic Algorithm: NSGA-II”, IEEE Transactions on Evolutionary Computation, vol. 6, no. 2, pp. 182-197, Apr. 2002.

[19] Vacuumschmelze. Available on line http://www.vacuumschmelze.com/, accessed on March 17 2018.

[20] JFE steel corporation. Available on line, http://www.jfe-steel.co.jp/, accessed on March 17 2018.

[21] Brest, J., Greiner, S., Boskovic, B., Mernik, M., Zumer, V. “Self- adapting control parameters in differential evolution: A comparative study on numerical benchmark problems”. IEEE Transactions on Evolutionary Computation, vol. 10, no. 6, pp. 646–657, Dec 2006.

[22] Infolytica. Available online: http://www.infolytica.com/, accessed on March 17 2018.

[23] Ansys. Available online: https://www.ansys.com/, accessed on March 17 2018.

[24] Russell, R. L., Norsworthy, K. H.: “Eddy currents and wall losses in screened-rotor induction motors”. Proceedings of the IEE - Part A: Power Engineering, vol. 105, no 20, pp. 163 – 175, Apr 1958.